Effects of Biodynamic Coupling on the Human Operator Model

M. Idan*
Stanford University, Stanford, California 93405
and
S. J. Merhav†
Technion—Israel Institute of Technology, Haifa, 32000 Israel

Describing function models of the human operator in manual tracking tasks developed so far have essentially been restricted to a static cockpit environment using fixed based simulators. This paper addresses the problem of whether, and how, the response of the human operator and his associated describing function are influenced by cockpit motion induced by his own control commands. It is suggested that the motion-induced biodynamic stick feedthrough affecting the inner kinesthetic control loop can be interpreted as a modification of the dynamics of the controlled vehicle. By assuming that the crossover model remains valid under conditions of vehicle motion, an extended analytical model of the human operator describing function is derived. Computer simulation of this analytical model provides reference characteristics of the describing function and remnant noise. A validation of this model, accomplished by extensive dynamical tests on a moving base simulator, is described. The excellent match of the analytical and experimental characteristics obtained both in magnitude and shape substantiates the notion of the extended human operator model and suggests that it may contribute to improved overall pilot-aircraft system design.

I. Introduction

A PILOTED aircraft is one of the most significant examples of a man-machine system. The aircraft response to pilot commands is influenced by their mutual tight interaction. An aircraft with good stability characteristics per se does not necessarily ensure good handling qualities.[1] This property involves not only the response of the aircraft to pilot commands but also the dynamical response of the pilot to the aircraft accelerations.

The human operator in a man-machine system can be described as an optimal adaptive controller with certain inherent psychophysical limitations. This idea has produced a large volume of theoretical and experimental studies in the area of human operator (HO) and man-machine models. The first models were based on classical frequency domain control theory and described the HO in single-axis tracking tasks.[2] The adaptation of the HO manifests itself by the adjustment of his mode of control in accordance with the particular dynamical characteristics of the controlled element. During control activity, the human operator senses, in addition to visual information, kinesthetic stimulation, or "motion cues," by means of the vestibular system,[3] and neuromotor motion and force sensors.[4] The effect of the motion cues on HO performance was studied by Stapleford et al.[5] on moving base simulators. These studies disclosed that, by and large, motion cues improve HO control performance. In extreme cases, the absence of the motion cues can lead to pilot-induced oscillations (PIO). The optimal behavior of the HO motivated further work on HO modeling by Kleinman et al.,[6] who adopted an approach of modern optimal control theory.

In actual flight missions, the pilot is often subjected to accelerations and vibrations that cause biodynamic interferences. These interferences cause nonvoluntary manual commands and tend to increase the remnant noise.[7] Motion and vibration also affect vision because the appearance of displays may become blurred.

If the vehicle accelerations are uncorrelated with the pilot's voluntary commands, the biodynamic interference is "open-loop," as is the case when a weapon is aimed onboard a helicopter. Open-loop biodynamic interference has been intensively studied by, among others, Allen[8] and Levison et al.[9,10] These investigations disclosed that remnant noise increases and nonvoluntary control commands can seriously affect tracking precision. These studies also led to the development of mathematical models of the biodynamical mechanism.[8,11,12]

In the course of the past two decades, a number of the methods aimed at reducing the effects of biodynamic interference were attempted. One recent approach is based on adaptive noise suppression techniques.[13] This method demonstrates substantial reduction in the effects of open-loop biodynamic interferences.

In piloted aircraft, the HO is subjected to accelerations resulting from his own commands. The resulting biodynamic interference will be referred to as "closed-loop," the effect of which may increase the originally intended control command and cause uncontrolled oscillations. This phenomenon, occurring in certain flight conditions,[14] is also known as pilot-coupled oscillations (PCO).

The purpose of this study is to develop a man-machine model incorporating closed-loop biodynamic effects. For the sake of simplicity, the controlled plant was modeled as a single integrator. The inclusion of the biodynamic feedthrough paths constitutes an extended HO model. This model incorporates the effect of motion on the performance and stability of the complete man-machine system. In this study, a theoretical model is developed that is validated by motion flight simulation experiments.

II. Extended Human Operator Model

Background

Existing models of the HO in manual control tasks have been developed largely by experimental studies, using fixed based simulators. In these studies, the sole task-oriented infor-

Received Sept. 8, 1987; revision received March 28, 1989. Copyright © 1989 by the American Institute of Aeronautics and Astronautics, Inc. All rights reserved.

*Graduate Student, Department of Aeronautics and Astronautics. Student Member AIAA.

†Professor, Department of Aeronautical Engineering. Member AIAA.

mation displayed to the pilot is visual. Typical tasks have been the tracking of a random stationary zero-mean moving target. Eventually, it has become clear that models derived under these conditions only partially represent HO performance. Later work incorporated motion cues detected by the vestibular and neuromuscular systems.[5,7,15]

In addition, motion can induce biodynamic interference which is, in essence, uncontrolled response of human limbs to vibration and acceleration. Two kinds of interference are distinguished:

1) "Open-loop" biodynamic interference occurring in controlling and aiming of devices onboard moving platforms.

2) "Closed-loop" biodynamic interference, caused by vehicle accelerations, which is fed back to the manipulator and adds to the voluntary command.

In both cases, deterioration of the control performance of the HO occurs.

An HO model, based on classical control theory is presented in detail in Ref. 2, where the approach is based on a quasilinear time-invariant man-machine model shown in Fig. 1. The HO is described by the linear describing function Y_p and additive remnant noise n. The HO controls Y_c, which represents the plant; r is the plant output in response to the input c. Only the error $e = c - r$ is displayed to the HO. Extensive experimental investigation disclosed that Y_p can be described by the transfer function,

$$Y_p(j\omega) = K_p \frac{e^{-j\omega\tau}}{j\omega T_N + 1} \frac{j\omega T_L + 1}{j\omega T_I + 1} \tag{1}$$

where $e^{-j\omega\tau}$ is the effective time delay of the HO, $1/(j\omega T_N + 1)$ is the neuromuscular lag, and $G(j\omega) = (j\omega T_L + 1)/(j\omega T_I + 1)$ is an equalization term that enables the adjustment of the model to a wide variety of plant models $Y_c(j\omega)$.

In the numerous experiments that have been performed,[2] the adaptive nature of Y_p has been established. The adaptation takes place in accordance with the crossover model, stating that the overall transmission Y_pY_c maintains a slope of -20 dB/dec in the region of the gain crossover, and it is given by

$$Y_pY_c(j\omega) = \frac{\omega_c}{j\omega} e^{-j\omega\tau} \tag{2}$$

The "compensation network" $G(j\omega)$ adjusts itself adaptively so that Eq. (2) holds for a variety of plants Y_c. The crossover frequency ω_c, along with phase margins and input bandwidth, is an important parameter in the determination of the man-machine system performance.

The remnant noise $n(t)$ is defined as that portion of the HO control signal that is uncorrelated with $c(t)$. In accordance with Ref. 2, the origin of $n(t)$ is the nonstationarity of the parameters of the HO.

Consistent with earlier work, the proposed model in this study is based on the adaptive nature of the HO. The underlying assumption is that he adjusts his response so that the crossover model of the man-machine system holds in the presence of closed-loop biodynamic interferences.

The models of biodynamic interference developed so far[8,11,12] addressed problems with external disturbances, i.e., open-loop biodynamic interference. Specifically, the studies performed addressed the effects of high-frequency vibrations on manual manipulator tasks. In these models, the various body limbs are described by lumped dynamical models consisting of masses, inertias, springs, and dampers. The range of frequencies in which experiments were performed was relatively high, i.e., greater than 1 Hz. In this frequency range, the feedthrough to the stick has a distinct low-pass nature, with a break frequency near 5 Hz.[8] This characteristic stems mainly from the bob weight effects of the body limbs and especially the hand gripping the stick. The reason for this phenomenon is that the HO does not respond in the high-frequency range beyond approximately 1 Hz. Consequently, intereference components in this frequency range add directly to the voluntary control.

In principle, low-frequency components of biodynamic interference should also be considered in the HO modeling. The implication would be that, e.g., under constant acceleration, such as flight with sideslip, the pilot would lean on the stick and would cause a tracking error. In reality, the HO compensates such errors reflexively without difficulty. From the foregoing it can be argued that the HO response is influenced by the existence of low-frequency biodynamic interference. This influence should manifest itself by a modification of the HO describing function in the low-frequency range.

Modeling of Biodynamic Interference

Previous models[8,11,12] describe the biodynamic interference as a low-pass nonvoluntary response to accelerations, adding to the voluntary control commands. This nature of biodynamic interference has been observed in experiments[9] in which the excitation frequencies were above 1 Hz. In the low-frequency range, if constant accelerations exist, the HO easily manages to compensate them reflexively and to reduce their effect by adjusting his grip on the control stick. This reflexive compensation is effective, particularly in the low-frequency range, in which the HO can easily estimate motion and disturbances. This range is limited by the bandwidth of the associated vestibular and neuromotor motion sensors. In this study, it is therefore assumed that the pilot response to accelerations and vibration, being of a reflexive nature, has a high-pass-type describing function at low frequencies and, as a result of natural low-pass roll-off, it has a low-pass nature at high frequencies. Consequently, the overall HO biodynamic response has a band-pass-type describing function. A block diagram describing this model is given in Fig. 2, in which the following notations apply: Y_p, HO model describing desired response to visual input; Y_k, kinesthetic model describing neurosensor response; Y_b, model of the passive biodynamic transmission; Y_n, model of neuromuscular system describing manual control commands; a, acceleration; e, tracking error; u_c, voluntary control command of the HO; n, remnant noise; u_b biodynamic feedthrough signal to control stick; u, total control command.

The model introduced here, though having a reasonable basis, requires experimental validation. A straightforward validation would be feasible if it were possible to measure the HO response to accelerations and vibrations and to separate it into

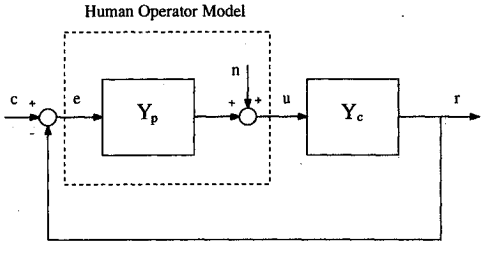

Fig. 1 Man-machine system for a compensatory tracking task (after McRuer et al.[2]).

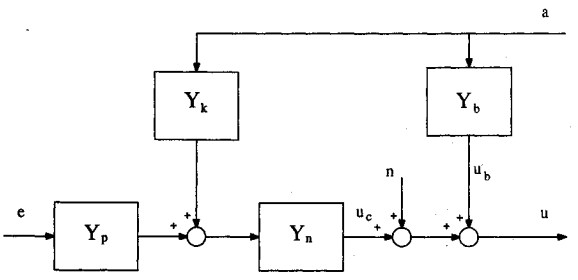

Fig. 2 Model of human operator response to accelerations and vibrations.

its two components, i.e., the nonvoluntary component and the reflexive one. Such a separation is not practical. Therefore, in this study, the validation of the closed-loop biodynamic model is performed by overall system model matching techniques described in Sec. III.

Effects of the Biodynamic Feedthrough

In view of the foregoing, the description of the biodynamic interference is governed by a combination of the nonvoluntary feedthrough commands and the reflexive compensation response. If the vehicle sensed by the HO is due to his own commands, a biodynamic feedback path is established. A block diagram describing the HO in a tracking task incorporating biodynamic feedback is shown in Fig. 3. The following notation applies in this description: Y_c, model of the controlled plant; Y_p, model of the HO; Y_B, model of the total biodynamic transmission given by $Y_B = Y_b + Y_k Y_n$; c, system input; e, tracking error; u_c, voluntary command in the man-machine system; n, remnant noise; u_B, total response to acceleration fed through to the control stick; u, total control command; r, plant response; a, acceleration sensed by the HO.

As a result of the excitation c, a tracking error e develops. The HO attempts to minimize e by control commands u_c. The corresponding vehicle response r shows in the display and manifests itself by vehicle accelerations a, evoking u_B via Y_B, adding to u_c and n to provide u. These accelerations also have a direct effect on the HO, causing increased observation and motor noise.[7] The motion also has the effect of modifying the HO transfer function as explained later in this section.

If indeed the biodynamic feedback path Y_B exists, as shown in Fig. 3, its effect is as if the HO does not control the original plant Y_c but rather an equivalent system, which is modified by Y_B. Thus, we have an extended Y_c', given by

$$Y_c'(s) = \frac{r}{u_c}(s) = \frac{Y_c(s)}{1 - Y_c(s)Y_B(s)(a/r)(s)} \tag{3}$$

From Eq. (3), the equivalent system Y_c' is determined by Y_c, Y_B, and the transfer function a/r. Y_c' may be strongly affected by variations in Y_B, and it depends on the particular form of a/r, which is determined by the specific force and by the distance between the center of rotation and the location of the HO.

In the present study, the concept of the extended model in Eq. (3) is validated by means of a three-degree-of-freedom moving base simulator, allowing pitch, roll, and heave motion. The simulator cabin is suspended from a two-axis cardan joint, located at a distance L above the elbow of the HO, providing pendulous motion in pitch and roll. A detailed description of this simulator is given in Ref. 13. The experiments described later were limited to lateral angular motion, thus evoking side forces only.

The effect of the biodynamic feedthrough on Y_c' was studied by means of the following example.

The controlled system Y_c was chosen as K_c/s, with $K_c = 20$ $(\text{mm/s}^{-1})/\text{N}$. The transfer function a/r is determined by the particular configuration of the simulator used in this study. The translatory lateral specific force sensed by the HO is given by $L\ddot{\phi}$, where ϕ is the roll angle, and by the lateral gravity component $g \sin\phi$, which opposes $L\ddot{\phi}$. As a result of these pendulous opposing forces, there exists a frequency $s = \pm j\sqrt{g/L}$ at which no lateral specific force is sensed at the HO elbow level. In other words, the transfer function from the simulator motion input r given by the response of Y_c to the sensed lateral specific force a has a pair of imaginary zeros at that frequency. Considering also the dynamics of the drive system, which is modeled as a second-order dynamical system,

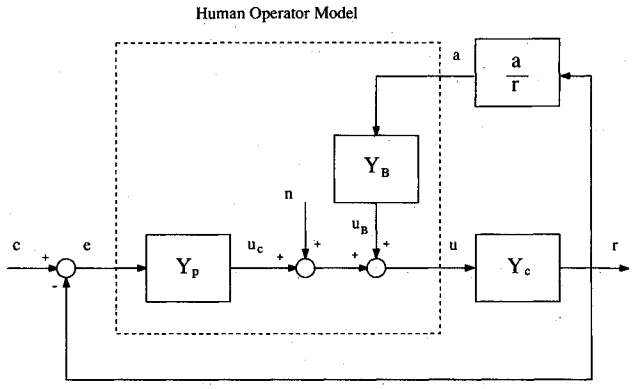

Fig. 3 Closed-loop biodynamic feedthrough in man-machine system.

the transfer function a/r is given by

$$\frac{a}{r}(s) = K_a \frac{(s^2 + g/L)\omega_s^2}{s^2 + 2\zeta_s\omega_s s + \omega_s^2} \tag{4}$$

where K_a, ζ_s, and ω_s describe the dynamics of the simulator drive system. The numerical values in Eq. (4) are: $L = 1$ m, $g = 9.81$ ms^{-2}, $\omega_s = 8$ rad/s, $\zeta_s = 0.3$, and $K = 0.0065$ $(\text{ms}^{-2})/\text{mm}$.

In accordance with Sec. II, the transfer function Y_B is modeled by

$$Y_B(s) = K_B \frac{s}{s + b_h} \frac{b_l}{s + b_l} \tag{5}$$

The first factor in Eq. (5) is the high-pass term. The values of K_B and b_h, initially not known, depend on a variety of factors, such as physical properties of the HO, his posture, and the manner in which the stick is gripped. Typical values of K_B and b_h, as shown later, were found to be $K_B = 3$ N/g and $b_h = 0.7$ rad/s. The low-pass term, in accordance with Allen et al.[8] and Levison et al.,[9] is chosen as $b_l = 30$ rad/s.

Equations (4) and (5) determine the open-loop transfer function $Y_B Y_c(a/r)$ shown in Fig. 3, namely,

$$Y_B(s)Y_c(s)\frac{a}{r}(s) = K_B \frac{s}{s + b_h}\frac{b_l}{s + b_l} K_a \frac{(s^2 + g/L)\omega_s^2}{s^2 + 2\zeta_s\omega_s + \omega_s^2}\frac{K_c}{s} \tag{6}$$

The magnitude and sign of the product $K_B K_a K_c$ determine the location of the closed-loop poles of the extended system Y_c'. The sign of the biodynamic feedthrough is determined by a/r. If, for example, the roll motions are around an axis above the HO's head, as could be the case in a helicopter or in the motion simulator used in the tests in this study, the sign of the preceding product is positive. Conversely, if the axis of rotation is below the HO, the sign is negative. For the values of the parameters of Y_c, a/r, and Y_B, the zeros and poles of the open-loop transfer function in Eq. (6) assume the following values:

$$Y_B(s)Y_c(s)\frac{a}{r}(s) = \left[\frac{K_B K_a K_c}{s}\right]\left[\frac{s}{s + 0.7}\right]\left[\frac{30}{s + 30}\right]\left[\frac{64(s \pm 3.16j)}{s + 2.4 \pm 7.6j}\right] \tag{7}$$

The location of the poles of Y_c' as a function of the gain $K_B K_a K_c$ is shown in Fig. 4. It is clearly seen that three of the poles tend to move toward the imaginary axis and that, for a sufficiently large gain, Y_c' becomes unstable. In accordance with Eq. (3), its specific form is given by

$$Y_c'(s) = \left[\frac{K_c}{s}\right]\left[\frac{(s + b_h)(s + b_l)(s^2 + 2\zeta_s\omega_s s + \omega_s^2)}{(s + b_h)(s + b_l)(s^2 + 2\zeta_s\omega_s s + \omega_s^2) - K_c K_B K_a b_l \omega_s^2 (s^2 + g/L)}\right] \tag{8}$$

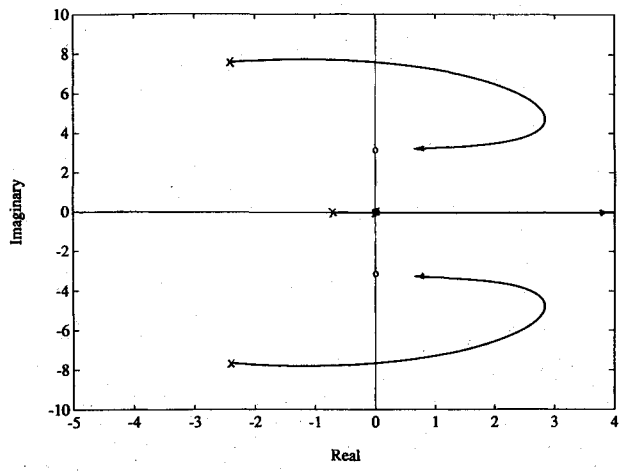

Fig. 4 Root-locus of the modified plant Y_c' as a function of the biodynamic feedback gain.

The second factor in Eq. (8) represents the modification of $Y_c = K_c/s$ to Y_c' as a result of the biodynamic feedthrough. Equation (8) indicates that the transfer function Y_c has assumed a more complex form which, for sufficiently large values of $K_BK_aK_c$, can present a more difficult manual control task. For the numerical values given earlier, Y_c' is given by

$$Y_c' = \frac{20}{s}\frac{(s+0.7)(s+30)(s+2.4\pm 7.6j)}{(s+0.29)(s+32.6)(s+1.3\pm 7.8j)} \tag{9}$$

In the present example, Y_c' given by Eq. (9) indicates only a moderate modification of Y_c as a result of the low values of $K_BK_aK_c$. Yet this difference can cause a noticeable change in the frequency response characteristics of Y_p, in the present example, particularly at the low-frequency range. If such a change can be validated by dynamic simulation experiments with sufficient confidence, the hypothesis for the proposed modification of Y_c to Y_c' will be established.

III. Experimental Validation

The purpose of the experimental program is to validate the analytical model presented in Sec. II. Its philosophy is guided by the following assumptions and considerations:

1) In the closed-loop system, as shown in Fig. 3, only the total control u is measurable and, since u_B and u_c are correlated, it is not possible to identify $Y_B(s)$ from the measurements taken in closed-loop tests.

2) If, however, $Y_B(s)$ were known a priori, the concept of the modified controlled element $Y_c'(s)$, as given in Eq. (3), could be validated.

3) In the open-loop biodynamic case, as defined in Sec. II, $Y_B(s)$ can readily be identified by standard methods of spectral analysis. This is so because the tracking commands u_c are uncorrelated with the external accelerations.

4) In order to facilitate the modeling of $Y_c'(s)$ as defined in Eq. (3), it is here assumed that $Y_B(s)$ in the open-loop case is essentially the same as in the closed-loop case.

5) The rationale is that if this assumption is essentially correct, this model of $Y_B(s)$ derived by open-loop tests can be incorporated in the closed-loop model for $Y_c'(s)$.

6) Computer simulations incorporating this $Y_B(s)$ are carried out for the extended model given in Eq. (8). These simulations are planned to yield reference model power density spectra and the open-loop describing function.

7) Actual motion simulator tests with human subjects are processed to yield corresponding power spectra and the describing function. The comparison of these functions with the ones computed from the reference model response is the rationale for the validation of the concept of the extended HO model defined by $Y_c'(s)$. If a good match is obtained, the a priori unsubstantiated assumption 4 can also be considered valid.

Experimental Setup

The experimental work was carried out on a three-degree-of-freedom moving base simulator. The cabin is suspended from three rods that are driven by dc torque motors, and it is hinged to a central column, which balances the cabin's weight by pneumatic pressure. The collective or differential motion of the driving rods provides pitch, roll, and heave motions of the cabin. A detailed description of the simulator is given in Ref. 13.

The cabin is equipped with an aircraft ejection-type seat, an isomorphic two-axis force stick such as the one used in the F-16, and a 9-in. raster display on which the tracking task is displayed to the HO. Three accelerometers measure the cabin accelerations. The cabin windows are opaque in order to block the undesirable visual cues of the laboratory environment.

Two interconnected minicomputers were part of the experimental setup. One performs the two-way communication between the analog sensors of the simulator, as well as the computation of the simulator digital control. The second computer performs the simulation of the target motion and generates, in conjunction with a graphic translator, the dynamic display observed by the HO. It also handles the data acquisition and the processing of the experimental results.

Description of the Tracking Task

For the sake of simplicity, the control task was confined to lateral compensatory tracking. The tests were carried out in two categories: static tests, i.e., no motion, and motion tests, i.e., with lateral swing of the simulator cabin. Two kinds of dynamic experiments were performed:

1) "Open-loop" biodynamic tests, with external random excitation of the simulator, in which the controlled element Y_c represented, e.g., an electro-optical sensor manually controlled onboard a randomly moving or vibrating platform. The purpose of these tests was to investigate Y_B and to validate its bandpass nature, as assumed in Sec. II.

2) "Closed-loop" tests, in which the simulator motion was excited by the response of Y_c to manual HO commands. The purpose of these tests was to investigate the effects of closed-loop biodynamic interference on the HO model.

In all these tests, the dynamics of the controlled plant was represented by $Y_c(s) = K_c/s$, which was simulated in the computer at the frame rate of 100 Hz. K_c was set to 20 (mm/s^{-1})/N. The data acquisition was performed every six time frames, i.e., at the rate of 16.667 Hz.

The display presented to the HO was a plus sign and a multiplication sign. The "+," fixed in the center of the screen, represented the direction of the line of sight of the electro-optical device or, alternatively, the direction of the fixed aircraft sight. The "×" represented the maneuvering target as it appeared in the field of view of the electro-optical device or in the aircraft sight, as the case may be. The deviation of the "×" from the "+" represented the tracking error e. The task of the HO was to minimize e by "moving" the "×" toward the center of the "+" by manual commands.

The experiments performed can be classified as follows:

1) Experiments to test the HO response to open-loop accelerations and vibrations (designated as configuration I). The target motion was generated in the computer by passing zero-mean Gaussian white noise through a second-order filter with a bandwidth of 1 rad/s and a damping factor of 0.7. The standard deviation of the target motion was 3 mm. The duration of an individual test was 260 s. Recording of the data started 15 s after the beginning of the test in order to reduce the effects of possible initial transient phenomena. Each subject carried out 24 statistically identical runs. The cumulative time for each subject therefore was approximately 100 min.

2) Tests to investigate the effects of closed-loop biodynamic interference on the HO performance (designated as configura-

tions II and III). Configuration II represents static tests, whereas III represents motion simulation experiments. In these tests, the target motion was identical to that of configuration I, with a standard deviation of 8.5 mm. The duration of each run was 260 s. Recording of the data started 15 s after the beginning of the test as before. Each subject performed 10 statistically identical runs. The cumulative time for each subject, therefore, was appoximately 41 min. During these experiments, it was noted that some of the subjects developed a strategy to reduce the effects of biodynamic interference by relaxing their grip on the control stick, so that the tracking error was still acceptable and the effect of the disturbances was reduced. To avoid this contrivance, a slowly varying external signal, representing, e.g., a random drift in the null point of the control stick, was added, thus forcing the HO to maintain his grip.

Simulator Motion

In the dynamic tests, the simulator performed pendulous roll motion, thus generating lateral accelerations.

Random simulator motion for the investigation of open-loop biodynamic interference was generated in the computer by passing zero-mean Gaussian white noise through a second-order filter with a natural frequency of 0.7 rad/s and a damping factor of 0.7. The filter output was fed into the simulator control system.

In the closed-loop biodynamic interference tests, the response of Y_c to HO control commands drove the simulator. The motion of the simulator was accompanied by corresponding changes in the display. The signal representing the response of Y_c was multiplied by a motion constant K_m and was fed into the drive system. The larger K_m, the larger the cabin motion for a given manual control command.

Subjects in the Tests

Four subjects participated in the tests. They were all students in the aeronautical engineering department. Their ages were 23–25. One subject had actual flight experience in light aircraft, and one had glider flight experience. All of the subjects had considerable experience on a fixed base simulator and tens of hours on the dynamic simulator, performing tests similar to the ones in the present study.

In each session, which lasted approximately 1 h, the subject executed about 10 runs of 260 s each. The subjects could rest between runs at their request. Prior to the experiment series, each subject underwent a training period until he reached a constant level of performance. Because of the considerable skill of the subjects, only short training periods of about 1 h were needed in order to change experimental configurations. Three subjects participated in each configuration.

IV. Analysis of the Experimental Results and Model Validation

The results of the experiments are shown in Figs. 6–12, including power spectrum densities and estimated describing functions. The analysis presented is in accordance with the objectives in Sec. II.

Identification of the Open-Loop Biodynamic Model

The identification of the open-loop biodynamic model Y_B, as presented in Sec. II, is a prerequisite to the identification of the closed-loop biodynamic model. For this purpose, experiments for configuration I were performed.

The program for data processing included the estimation of the HO describing function Y_p and the overall describing function Y_B of the HO response to acceleration. This was achieved by estimating the appropriate auto- and cross spectra of input and output variables. The various power spectrum estimates were computed by the method of modified periodograms of Welch.[16]

The man-machine system model, which underlies the data processing for this case, is shown in Fig. 5, with notation identical to that of Fig. 3. The measurable variables are c, e, u, a, and r only. The relationship between the response u and the error e, respectively, and the inputs c, a, and n is given by

$$u(s) = \frac{Y_p}{1 + Y_pY_c}\,c(s) + \frac{Y_B}{1 + Y_pY_c}\,a(s) + \frac{1}{1 + Y_pY_c}\,n(s) \tag{10}$$

$$e(s) = \frac{1}{1 + Y_pY_c}\,c(s) - \frac{Y_cY_B}{1 + Y_pY_c}\,a(s) - \frac{Y_c}{1 + Y_pY_c}\,n(s) \tag{11}$$

Since there is no correlation betwee the inputs c, a, and n, Eqs. (10) and (11) lead to

$$Y_p(j\omega) = \frac{\Phi_{uc}(j\omega)}{\Phi_{ec}(j\omega)} \tag{12}$$

$$Y_B(j\omega) = \frac{\Phi_{ua}(j\omega)}{\Phi_{ec}(j\omega)}\,\frac{\Phi_{cc}(j\omega)}{\Phi_{aa}(j\omega)} \tag{13}$$

In the preceding expressions $\Phi_{ij}(j\omega)$ are power spectral densities (PSD). The emphasis is on the identification of Y_B, which is the describing function relating the external accelerations and the nonvoluntary manual control.

The hypothesis for the bandpass nature of Y_B has been presented in Sec. II. Because of dynamic limitations of the simulator, it was not possible to evaluate the low-pass nature of Y_B beyond 3 Hz. This is not a serious shortcoming because this frequency range has been extensively studied by a number of investigators, e.g., Allen et al.[8] Therefore, in the present study, the emphasis is on the identification of Y_B in the low-frequency range which, in accordance with the assumptions in this study, has the nature of a high-pass filter, Eq. (5).

Two provisions were made to facilitate the identification in the low-frequency region:

1) The bandwidth of the random accelerations was made low so that most of their energy was confined to the low-frequency range.

2) Numerous runs were performed, with a cumulative time of 100 min for each subject.

The length of the data window for the identification of the various PSD functions was 16,384 points. This enabled reliable estimation down to the frequency of 0.0064 rad/s, with increments of 0.0064 rad/s.

A plot of the average gain of Y_B for the three subjects who participated in each of these tests is given in Fig. 6. The high-pass nature of Y_B is clearly distinguishable, with a break frequency of about 0.7 rad/s.

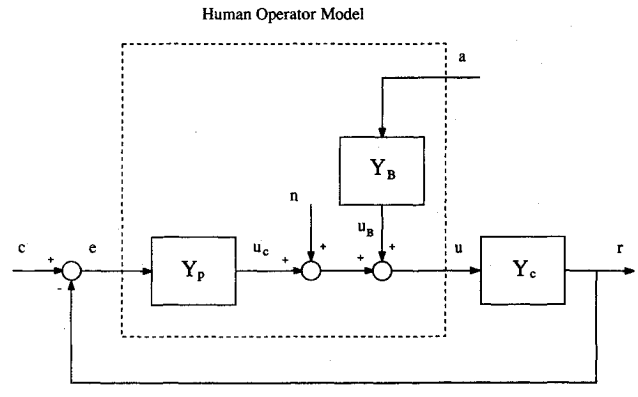

Fig. 5 Man-machine model for configuration I.

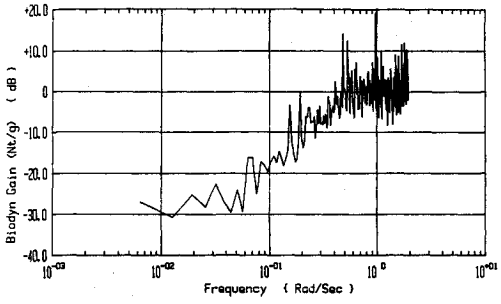

Fig. 6 Gain of the average biodynamic function Y_B: configuration I.

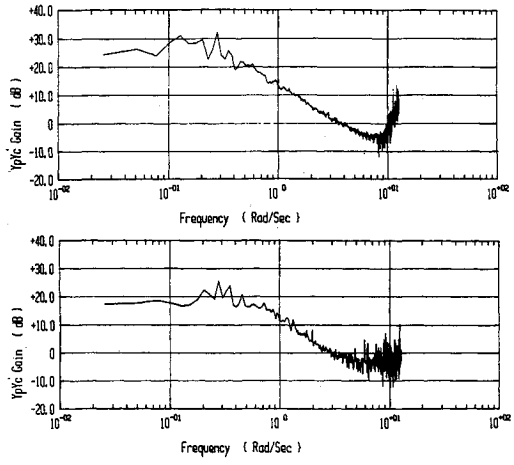

Fig. 7 Gain characteristics of Y_pY_c': a) configurations II, static test; b) configurations III, dynamic test with $K_m = 6.5 \cdot 10^{-3}$ rad/mm.

As stated earlier, it was not possible to identify the high-frequency breakpoint b_h of Y_B. Therefore, its value was set to 30 rad/s, using the results of previous investigations.[8] Consequently, Y_B was found to be

$$Y_B(s) = K_B \frac{s}{s + 0.7} \frac{30}{s + 30} \tag{14}$$

where the gain K_B is approximately 1 N/g. It should be borne in mind that K_B varies in accordance with the vibration level of the controlled plant.

Identification of the HO Model in a Closed-Loop Biodynamic Situation

A model of the man-machine system in the closed-loop biodynamic case was presented in Sec. II, Fig. 3. As stated in Sec. III, a slowly varying external signal was added to the stick output to shift its null point, thus ensuring that the HO maintains his grip during vibrations. This low-energy signal has almost no effect on the identification process in the frequency range of interest. Its main effect is on Y_p in the low-frequency range, as will be shown later.

The man-machine model shown in Fig. 3 has two unknown describing functions, Y_p and Y_B. Since there exists only one significant input signal c in the system, a straightforward identification of the two describing functions is impossible. Therefore, the method of model matching as adopted, as indicated in Sec. III.

First, the open-loop describing function Y_pY_c' was estimated, using the relation

$$Y_pY_c'(j\omega) = \frac{\Phi_{rc}(j\omega)}{\Phi_{ec}(j\omega)} \tag{15}$$

Further, the PSD of the control signal u, $\Phi_{uu}(j\omega)$, was estimated to determine the overall closed-loop man-machine describing function.

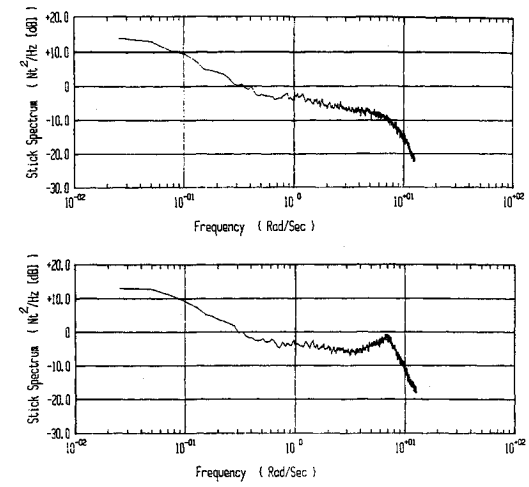

Fig. 8 Power spectra of the stick output u: a) configurations II, static test; b) configurations III, dynamic test with $K_m = 6.5 \cdot 10^{-3}$ rad/mm.

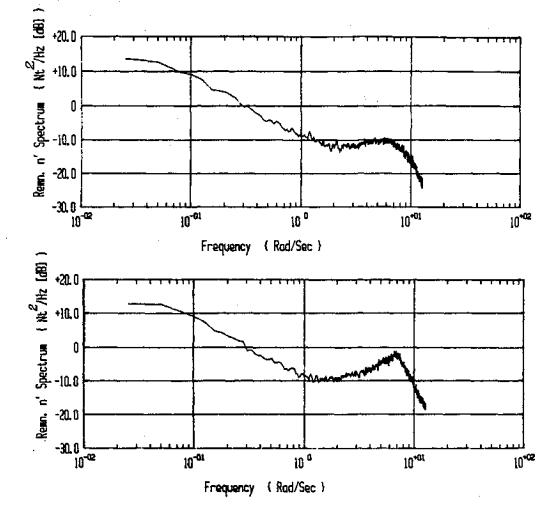

Fig. 9 Power spectra of the control component n': configurations II, static test, b) configurations III, dynamic test with $K_m = 6.5 \cdot 10^{-3}$ rad/mm.

The plots of the average gain characteristics of Y_pY_c' for the three subjects in test configurations II and III are shown in Figs. 7a and 7b. The frequency responses demonstrate that the crossover model holds in these cases, particularly in the region of the crossover frequency ω_c. In the dynamic tests, only slight variations in ω_c with respect to the static tests are observed. This implies that the HO manages to adapt his response to maintain the crossover model and to maintain good closed-loop control performance. The crossover frequency of Y_pY_c' was found to be $\omega_c \approx 2.8$ rad/s. In the sequel, this crossover model will be used for matching the analytical model of Sec. II to the experimental results.

There is an increase in the tracking error in the dynamic tests as compared to the static ones. In the static case (configuration II), the average tracking error was $e_{RMS} = 3.8$ mm. In the dynamic (configuration III) case, the average tracking error was $e_{RMS} = 5.6$ mm, which is an increase of 47% over the static case. It should be noted that, in the tests with open-loop biodynamic interference, the corresponding increase in the tracking error was about three time larger then in the static tests.[13]

The plots of the average $\Phi_{uu}(j\omega)$ for the three subjects in test configurations II and III are shown in Figs. 8a and 8b.

These plots show that, in the dynamic tests, there is an increase in $\Phi_{uu}(j\omega)$ in the region of 4–10 rad/s, with a peak around 8 rad/s, in comparison with the static case. The presence of this peak indicates relative instability in this frequency range. An explanation for this can be found in the extended model Y_c' described in Eq. (9). From this expression, one can observe that the biodynamic "loop closure" establishes a pair of complex dipoles in this frequency range that, when excited, cause peaking near the corresponding frequency.

This excitation cannot be explained solely by the forcing function c because this signal has relatively little energy in the frequency above 1 rad/s. Therefore, the excitation of the undamped mode must be attributed to the human operator's control component n', which is uncorrelated to the input c. The PSD of n', $\Phi_{n'n'}(j\omega)$, can be estimated by

$$\Phi_{n'n'}(j\omega) = \Phi_{uu}(j\omega) - \frac{|\Phi_{uc}(j\omega)|^2}{\Phi_{cc}(j\omega)} \tag{16}$$

The plots of the average $\Phi_{n'n'}(j\omega)$ for the three subjects in test configurations II and III are shown in Figs. 9a and 9b. Superficially, $\Phi_{uu}(j\omega)$ and $\Phi_{n'n'}(j\omega)$ appear to be very similar. However, closer observation reveals that, in the frequencies around 8 rad/s, a difference of the order of 10 dB exists. In Figs. 9, the increase in $\Phi_{n'n'}(j\omega)$ around 8 rad/s is clearly indicated. This supports the assumption that the peaking in the PSDs is largely a result of n'. The relatively large PSD at low frequencies is actually the result of the low-frequency distrubance added to the stick, and it should not be attributed to the remnant noise spectrum per se.

The man-machine model shown in Fig. 3 was numerically simulated. The variables in this digital simulation are indicated by ( )*. Accordingly, Y_c^* was set to K_c/s, as in the experiments, and the gain was set to $K_c = 20$ (mm/s^{-1})/N. The transfer function a/r was given in Eq. (4). Recall that a fundamental assumption, made in Sec. III, is that Y_B is the same for the open-loop and closed-loop biodynamic cases. Therefore, Y_B modeled in the computer simulation was the one obtained in the open-loop motion tests, Eq. (14). In the extended controlled element Y_c', Eq. (8), the value of K_B will be obtained by matching the analytical model to the experimental results.

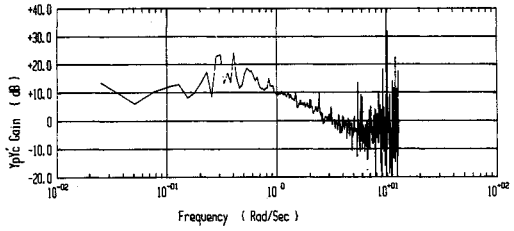

Fig. 10 Gain characteristics of $Y_p^* Y_c'$: model simulation results.

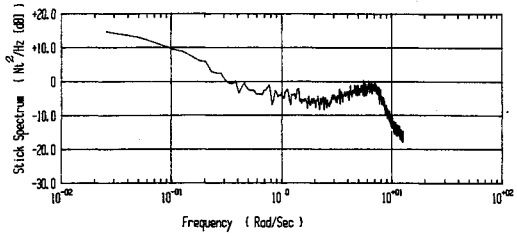

Fig. 11 Power spectra of the stick output u^*: model simulation results.

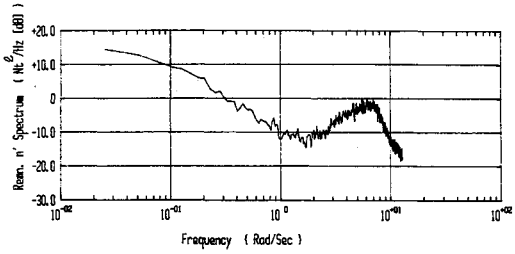

Fig. 12 Power spectra of the control component n': model simulation results.

As stated earlier, the HO adapts his response so that the crossover model holds, i.e., he provides the required phase lead to compensate for the lags in Y_c' at the frequencies below 1 rad/s. It is not plausible that the HO can provide compensation for the high-frequency dipoles in Y_c', as demonstrated in the example shown in Eq. (9). Therefore, in the computer simulation, Y_c^* was assumed to be of the form

$$Y_p^*(s) = K_p\left(1 + \frac{a_I}{s}\right)\frac{sT_L + 1}{sT_I + 1}\frac{1}{sT_N + 1}e^{-\tau s} \tag{17}$$

The parameters in Eq. (17) are the same as in Eq. (1). The proportional-integral control element $(1 + (a_I/s))$ was added to describe the HO response to the slowly varying signal added at the stick null point as described before. This modification is common in man-machine system models when a low-frequency signal exists. The simulation of the remnant noise n^* was obtained by passing Gaussian zero-mean white noise through a second-order low-pass filter.

The best fits between the analytical model response and the experimental results in configuration III were for the following parameters: $K_p = 0.022$ N/mm, $a_I = 0.4$ rad/s, $T_L = 10$ s, $T_I = 1.11$ s, $T_N = 0.2$ s, $\tau = 0.12$ s. The open-loop crossover frequency was $\omega_c^* = 2.8$ rad/s. The bandwidth of the remnant noise filter was 8 rad/s, with a damping factor of 0.7, and the rms of n was 1.31 N. The gain of Y_B was $K_B = 2.45$ N/g.

The gain characteristics of the simulated describing function $Y_p^* Y_c'^*$ are shown in Fig. 10. Comparison with the identified $Y_p Y_c'$ shown in Fig. 7b reveals a very good fit, particularly in the crossover region. The differences in the low-frequency range are typical and result from the relatively limited duration of the experiments and the corresponding computer simulation runs. The uncertainties in the identification in the high-frequency range are due to numerical limitations and particularly the relatively low energy of the excitation signal in this frequency region.

The PSDs of u^* and n'^*, estimated from the numerical simulation, are shown in Figs. 11 and 12, respectively. Comparison with the corresponding Figs. 8b and 9b from the experimental results indicates excellent matching.

Conclusions

The principal conclusions of this study are as follows:

1) The human operator model in manual tracking tasks is modified by the motion of the controlled vehicle.

2) The biodynamic interference at the control stick is of a bandpass nature.

3) The effect of motion can be viewed as a modification of the controlled plant, which is caused by the biodynamic feedback path. The adaptation required of the human operator manifests itself in additional low-frequency phase lead. An increase in the work load and a corresponding deterioration in the handling qualities can easily take place.

The testing of the proposed extended model was carried out for the case of manual control of a plant modeled as an integrator. This model does not present a particular aircraft. However, it represents the basic mode of rate control that is usually the design goal of control-augmented aircraft.

Although the dynamic flight simulator presented an unusual dynamical model, good correspondence between the results of the experiments and the computer simulated model was obtained.

The results of this study indicate that the notion of the extended model presented is a valid approach to more realistic man-machine system models involving dynamical pilot-aircraft interaction.

Acknowledgments

This work was carried out in partial fulfillment of the requirements for the degree of Master of Science at the Department of Aeronautical Engineering at the Technion—Israel Institute of Technology. The support of A. J. Grunwald during the initial phase of this work and the assistance of the technical staff of the Flight Control Laboratory are greatly appreciated.

References

[1]Harper, R. P., "Handling Qualities of Flight Vehicles," *Proceedings of the 25th Israel Annual Conference on Aviation ad Astronautics*, Haifa, Israel, Feb. 1983.

[2]McRuer, D. T., Graham, D, and Krendel, E. S., "Manual Control of Single-Loop Systems: Parts I and II," *Journal of the Franklin Institute,* Vol. 283, Jan.-Feb. 1967, pp.

[3]Hosman, R. J. A. W., and Van Der Vaart, J. C., "Vestibular Models and Thresholds of Motion Perception. Results of Tests in a Flight Simulator," Delft Univ., the Netherlands, LR-265, April 1978.

[4]McRuer, D. T., Magdaleno, R. E., and Moore, G. P., "A Neuromuscular Actuation System Model," *IEEE Transactions on Man-Machine Systems,* Vol. MMS-9, Sept. 1968, pp. 61-71.

[5]Stapleford, R. L., Peters, R. A., and Alex, F. R., "Experiments and a Model for Pilot Dynamics with Visual and Motion Inputs," NASA CR-1325, May 1969.

[6]Kleinman, D. L., Baron, S., and Levison, W. H., "An Optimal Control Model of Human Response, Parts I, II," *Automatica,* Vol. 6, 1970, pp. 357-373.

[7]Levison, W. H., Baron, S., and Junker, A. M., "Modeling the Effects of Environmental Factors on Human Control and Information Processing," AMRL TR-76-74, Aug. 1976.

[8]Allen, R. W., Jex, H. R., and Magdaleno, R. E., "Manual Control Performance and Dynamic Response During Sinusoidal Vibration," AMRL TR-73-78, Oct. 1973.

[9]Levison, W. H., and Harrah, C. B., "Biomechanical and Performance Response of Man in Six Different Directional Axis Vibration Environments," Aeromedical Research Laboratories, Wright-Patterson AFB, OH, AMRL TR-77-71, Sept. 1977.

[10]Levison, W. H., "Models for Human Controller Performance in Vibration Environments," *Aviation, Space, and Environmental Medicine,* Jan. 1978, pp. 321-327.

[11]Jex, H. R., and Magdaleno, R. E., "Biomechanical Models for Vibration Feed-through of Hands and Head for Semisupine Pilot," *Aviation, Space, and Environmental Medicine,* Jan. 1978, pp. 304-316.

[12]Riedel, S. A., Magdaleno, R. E., and Jex, H. R., "User's Guide to BIODYN-80: An Interactive Simulation Package for Modeling Biodynamic Feedthrough to a Pilot's Hands, Head and Eyes," System Technology Inc., Hawthorne, CA, Tech. Rept. 1146-1, Dec. 1980.

[13]Velger, M., Merhav, S. J., and Grunwald, A. J., "Effects of Adaptive Filtering in Manual Control on Board Moving Platforms," *Journal of Guidance, Control, and Dynamics,* Vol. 11, March-April 1988, pp. 153-158.

[14]Allen, M. G., "AFTI/F-16 Pilot Coupled Roll Oscillation," AIAA Paper 83-2232, Aug. 1983.

[15]Junker, A. M., and Levison, W. H., "Recent Advances in Modeling the Effects of Roll Motion on Human Operator," *Aviation, Space, and Environmental Medicine,* Jan. 1978, pp. 328-334.

[16]Welch, P. D., "The Use of Fast Fourier Transform for the Estimation of Power Spectra: A Method Based on Time Averaging Over Short, Modified Periodograms," *IEEE Transactions on Audio Electroacoustics,* Vol. AU-15, June 1967, pp. 70-73.

Recommended Reading from the AIAA Progress in Astronautics and Aeronautics Series . . . AIAA

The Intelsat Global Satellite System

Joel R. Alper and Joseph N. Pelton

In just two decades, INTELSAT—the global satellite system linking 170 countries and territories through a miracle of communications technology—has revolutionized the world. An eminently readable technical history of this telecommunications phenomenon, this book reveals the dedicated international efforts that have increased INTELSAT's capabilities to 160 times that of the 1965 "Early Bird" satellite—efforts united in a common goal which transcended political and cultural differences. The book provides lucid descriptions of the system's technological and operational features, analyzes key policy issues that face INTELSAT in an increasingly complex international telecommunications environment, and makes long-range engineering projections.

TO ORDER: **Write, Phone, or FAX:** AIAA c/o TASCO, 9 Jay Gould Ct., P.O. Box 753, Waldorf, MD 20604 Phone (301) 645-5643, Dept. 415 ■ FAX (301) 843-0159

Sales Tax: CA residents, 7%; DC, 6%. For shipping and handling add $4.75 for 1-4 books (call for rates for higher quanties). Orders under $50.00 must be prepaid. Foreign orders must be prepaid. Please allow 4 weeks for delivery. Prices are subject to change without notice. Returns will be accepted within 15 days.

1984 425 pp., illus. Hardback
ISBN 0-915928-90-6
AIAA Members $29.95
Nonmembers $54.95
Order Number V-93